Molecular BioSystems

Accepted Manuscript

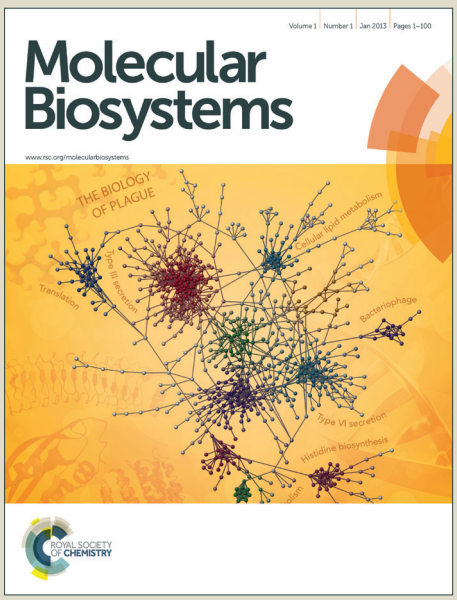

ROYAL SOCIETY OF CHEMISTRY

www.rsc.org/molecularbiosystems

Graphical abstract

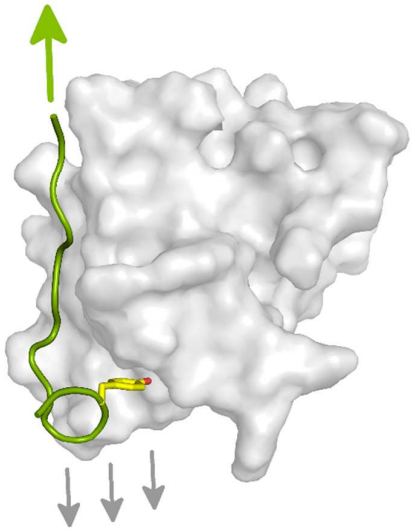

Interactions and force resistance of different β-integrin-talin complexes were analysed in a set of steered molecular dynamics simulations.

The talin-integrin interface under mechanical stress

Sampo Kukkurainen[a,b] , Juha A. Määttä[a,b], John Saeger[c], Jarkko Valjakka[a], Viola Vogel [c*] and Vesa P. Hytönen [a,b*]

[a] University of Tampere, BioMediTech, Tampere, Finland.

[b] Fimlab Laboratories Ltd., Tampere, Finland.

[c] Laboratory of Applied Mechanobiology, ETH Zurich, Zurich, Switzerland.

* Corresponding authors: VPH: vesa.hytonen@uta.fi, VV: viola.vogel@hest.ethz.ch

The major mechanical function of talin is to couple the β-integrin cytoplasmic tails to actin filaments. A variety of β-integrin tails contain conserved binding motifs for talin, and recent research shows that β-integrins differ both in affinity to talin and preferences for other cytoplasmic adaptor proteins. While talin predominantly links β3 integrins to actin filaments within the peripheral cell adhesion sites, talin can become replaced by other integrin adaptor proteins through their overlapping binding sites on integrin tails. Although the NPxY motif in the β-integrin tail is important for talin recognition, our simulations suggest considerably smaller contribution of the NPxY motif in the force resistance of the talin-integrin complex than for the residues upstream of the NPxY. It might thus be possible for the NPxY motif to detach from talin and interact with other integrin binding proteins while the β-integrin still remains bound to talin. The epithelial integrin β6 reportedly activates latent TGFβ1, and we propose that its function may involve direct interaction with talin.

Introduction

Cells sense and respond to the rigidity of their environment [1, 2], and the interactions with their surroundings control the molecular composition of adhesion complexes, cellular shape and movement [3-6]. Focal adhesions are complex structures containing cell membrane receptor integrins and more than 100 different proteins with signaling and scaffolding functions [7, 8] (Figure 1 A). They mediate cell attachment to the extracellular matrix (ECM), and transmit mechanical forces between the cytoskeleton and ECM [9, 10].

Integrins exist in conformations that differ in ligand binding ability. They form weak interactions with ligands in the ECM, and this induces integrin clustering and the recruitment of cytoplasmic adaptor proteins, such as talin [11]. Talin, in turn, contributes to the "inside-out" activation of integrin, and reshapes the contacts between the integrin transmembrane domains [12-16], possibly together with kindlin [17, 18]. This results in a conformational change that is transmitted from the integrin transmembrane segments to the extracellular domains, which then assume a high-affinity ligand binding conformation [19-22]. The integrin-bound talin functions as a scaffold that harbors other focal adhesion proteins, and links the integrin-matrix connection to the force bearing structures

of the cell by direct binding to actin filaments [23]. This scaffold is also the target of adhesion turnover regulation by calpain, which cleaves talin and thereby facilitates the disassembly of the adhesion [24, 25].

The initial interaction between the integrin-talin complex and actin is weak and breaks at 2 pN at a 60 nm s^{-1} loading rate [26, 27]. The ECM-actin contact grows in size and gains strength through the binding of other adhesion proteins, such as vinculin [28-31], and by the lateral association or clustering of integrins, particularly β1 [32-35]. Early integrin-ECM interactions and clustering may take place independently of the force generating machinery of the cell [11, 23, 28], but further steps of adhesion formation and maturation are regulated by tension between the ECM and the cytoskeleton [36, 37]. Within the cell, tensions are generated as actin assembly at the adhesion sites pushes the membrane outwards [6, 38, 39], and myosin-generated traction forces pull actin filaments inwards from the adhesion sites [6, 20, 40]. Moreover, substrate stiffness guides the adhesion processes [40]. Under tension between the ECM and cytoskeleton, the talin rod domain stretches and shortens cyclically [41]. In this process, the talin-integrin interface is exposed to mechanical load in the range of up to 30 pN at physiological loading rates [42], which is sufficient to expose buried vinculin binding sites in the talin rod domain and to thereby reinforce talin-actin binding [43-45].

Humans have 24 different integrins, each composed of one of 18 α chains and one of 8 β chains [19, 46]. In addition, alternative splicing has been found for example in β1 integrin [47-49]. Moreover, the two talins – talin-1 and talin-2 – may serve separate functions, as talin-2 knockout mice develop a myopathy [50], whereas a talin-1 knockout is embryonic lethal [51]. Talin-1 is known to bind β1-integrin variants β1A [52-55] and β1D [53-55], but also integrins β2 [56], β3 [12, 55, 56], β5 [56], and β7 [54, 57]. The talin-binding site in β-integrin cytoplasmic tails is composed of a membrane-proximal α-helix with conserved charged and aromatic residues, and a membrane-distal site with a conserved tryptophan (W739 in β3) and an NPxY motif (Figure 1 A, B). It has been proposed that the membrane-distal site provides the first contact to talin, followed by membrane-proximal α-helix binding and subsequent reorganization of the contacts between the α and β integrin transmembrane helices [15, 58, 59].

Integrins β1A, β1D, and β3 have different affinities for talin [55, 60], and show differences in binding conformation [55, 61]. Moreover, a recent report suggests that β1 and β3 integrins may have separate functions in adhesion [62], with β1 forming strong adhesions through clustering, and β3 functioning in mechanotransduction and binding only transiently to talin [35, 63]. The cytoplasmic domain of β-integrins also serves as a binding site for a number of other cytoplasmic proteins [64], among which at least α-actinin, filamin, and tensin also directly connect integrins to the actin cytoskeleton [65-67]. While talin predominantly links β3 integrins to actin filaments within the peripheral cell adhesion sites, α-actinin can replace talin through its overlapping binding site on integrin tails. α-actinin thereby contributes to the adhesion maturation, dynamic force generation and force release [68]. Filamin also competes with talin for β-integrin binding, and increased filamin binding blocks integrin activation by talin [54, 69]. Consequently, the sequence differences of β-integrins (Figure 1 B) and the

mechanical stability of the integrin-talin linkage may contribute to how adhesion site formation and breakage is regulated by mechanical signals.

The binding conformation of the membrane-distal site has been shown for the β3-talin-1 [61] complex, and of the membrane-distal and membrane-proximal sites for the β1D-talin-2 complex [55]. Yet, such structural knowledge of other β-integrins is not available. Moreover, what happens in integrin-talin complexes as they are exposed to mechanical load is poorly understood, leaving a gap in understanding of the force-regulated formation and maturation of adhesion sites. In an attempt to bridge this gap, we utilized all-atom molecular dynamics simulations to study the interactions in the membrane-distal talin binding sites - the presumed [15] first interactions between talin and integrin - of different β-integrins under tension between the extracellular matrix and the cytoskeleton.

β6 is among the less studied integrins, and has not been previously reported to bind talin-1. Integrin β6 is exclusively epithelial, generally downregulated in healthy cells and upregulated in tissue injury [70-72] and tumors (reviewed by Bandyopadhyay and Raghavan [73]). β6 has been shown to interact with kindlin-1 [74], a protein that assists talin in the activation of integrin [75], and studies show that β6 and talin-1 co-localize in focal adhesions [74, 76]. Moreover, latent TGFβ1 activation by αvβ6 has been shown to require a connection to both the ECM [77] and the cytoskeleton [78], suggesting a force-driven activation mechanism and a potential role for talin in the process. We were therefore intrigued to find that it formed a relatively stable complex with talin-1 in simulation, thus motivating us to study the binding of both β6 and our reference molecule β3 to talin *in vitro*.

Results and discussion

Initial conformations

The cytoplasmic domains of integrins β1A, β1D, β3, β5, β6, and β7 contain the key residues (W739(β3) [61] and NPxY [56]) required for interaction with talin-1 (Figure 1 B). As the structure of the β3-integrin cytoplasmic tail in complex with talin-1 is known (PDB ID: 1MK7 [61]), we utilized this structural information to model the talin-1 complexes of the six different β-integrins. Steered molecular dynamics (SMD) simulations using these complexes revealed how differences in β-integrin cytoplasmic tail sequences affect the stability of their complexes with talin. We first ran three 1-ns simulations without external force for each complex before starting the SMD pulling simulation. This was done in order to let the β3-talin-1 structure based models settle, and to obtain baseline trajectories. The baseline trajectories obtained from these simulations were analyzed by measuring the area of the talin-integrin interface, the number of hydrogen bonds between the integrin peptide and the talin head, and the root mean square fluctuation (RMSF) for Cα atoms (Table 1), and of the three structures obtained the one with the largest interface area and most hydrogen bonds was selected as the starting structure for the SMD simulations with external force. These baseline measurements showed that the initial

conformations were relatively stable for β3 and β5 peptide complexes with talin. Visual inspection of the complexes showed that β7 integrin peptide took a distinct, loosely bound conformation (Figure 1 C).

The crystal structure of the β1D-talin-2 complex (PDB ID: 3G9W [55]) shows a different talin binding conformation for the integrin peptide. This structure has been solved for talin-2 instead of talin-1, and it is unclear whether the same binding conformation would exist in talin-1. To address this question, we prepared another set of simulations for the β1A and β1D complexes, from here on called β1A-3G9W and β1D-3G9W, respectively, using the integrin conformation from the 3G9W structure but complexed with talin-1 from 1MK7. The baseline simulations without external force showed milder changes in the talin-1-integrin interface of β1A-3G9W and β1D-3G9W, compared to the interface of β1A or β1D prepared with the 1MK7 talin-1 structure. Moreover, the integrin-talin binding interface area was larger in β1A-3G9W and β1D-3G9W (Table 1).

Contact lifetimes in constant force pulling simulations

The complexes were subjected to constant force pulling in a set of molecular dynamics simulations using forces ranging from 200 pN to 600 pN. Several individual contacts in the talin-integrin interface contribute to the force resistance of the complex. The individual contacts were dynamically switching between bound and unbound states, and therefore their lifetimes do not have clearly defined endpoints. This is why we evaluated the force dependency of these contacts by measuring distances between selected atoms in the talin-integrin interface throughout the constant force pulling simulations. The distances were plotted as histograms showing the time in picoseconds spent at each distance (Figure 2 A-D). We then identified on-states for the contacts showing sharp peaks in the distance histograms, and estimated the lifetimes of these contacts by counting the observations of the contact within a defined cut-off distance (Figures S1-S4). Four contacts along the talin-integrin interface were used for this measurement. The packing of the side chain of the conserved integrin tryptophan residue with R358(tal) was assessed by measuring the distance between the centers of mass of the tryptophan and R358(tal) side chains (Figure 2 A). Next to the tryptophan residue, the D740(β3) and W359(tal) residues form 1-2 backbone hydrogen bonds with each other (Figure 3), and the distance between their Cα atoms was used as an indirect measure of this contact (Figure 2 B). The A742(β3) residue forms an additional backbone hydrogen bond to K357(tal) in some of the simulations (Figure 3 B), and this extended backbone hydrogen bonding was measured using the A742(β3)-K357(tal) Cα-Cα distance (Figure 2 C). Finally, the binding of the integrin NPxY tyrosine side chain to its binding groove was measured using the distance of the Y747(β3) side chain center of mass from the backbone carbonyl oxygen of N355(tal) (Figure 2 D).

The histogram of the D740(β3)-W359(tal) distance showed a sharp peak around 6 Å (Figure 2 B), which indicates the presence of a bound state. The Y747(β3)-N355(tal) forms a less pronounced peak (Figure 2 D), which reflects the less tight binding and the variety of conformations that the NPxY motif took in the simulations. For each simulation, the total time spent within a cutoff distance of 5 Å (Figure S1) or 7 Å (Figures S2-S4). Using the D740(β3)-W359(tal) distance as a measure (Figure 2 B), our results grouped β3, β5 and β6

together as forming the most stable complexes with talin, whereas β7 dissociated most rapidly. The talin complexes of β1A, β1A-3G9W, and β1D-3G9W all had short lifetimes, and β1D formed clearly more stable complexes than the other β1 peptides in the simulations.

The membrane-proximal site may function as a second binder after the first interaction with the membrane-distal site is formed [15], and its importance for talin binding has been estimated to be greater for β3 than for β1A integrin [60]. Although we excluded the membrane-proximal binding site from this study, β3 appeared to bind talin more tightly than β1A. According to previous reports [60], the affinity of β3 to talin-1 is slightly above that of β1A, with β1D having the highest affinity. Taken together, the membrane-distal site of β3 appeared to be more force-resistant in our simulations than one might predict from equilibrium affinities [60].

In the case of integrins β3, β5, and β6, individual 200 pN simulations and one 300 pN simulation showed particularly long (> 30 ns and approximately 17 ns, respectively) bound states. To identify the interactions that might account for the stability of the complex, we focused on the hydrogen bonding patterns of these simulations. Although the number of very stable (lifetime more than 50% of simulation length) hydrogen bonds in these simulations varied between 2 and 4, only one backbone hydrogen bond was common to all these simulations, namely the bond between D740(β3) amide group and W359(tal) carbonyl oxygen (Table 2).

Hydrophobic contacts

To evaluate to contribution of hydrophobic effect in the talin-integrin interaction under mechanical stress, we analyzed the buried area of hydrophobic residues within the interface (Figure S5). The buried hydrophobic area remained relatively constant in most simulations, and started to decrease as the hydrogen bonds along the talin-integrin interface were ruptured. The buried hydrophobic area of β1-talin complexes was clearly larger in the 3G9W-based simulations (~500 Å^2) than in the 1MK7-based simulations (~300 Å^2), but the 3G9W-based simulations failed to show greater force resistance. Furthermore, two simulations with a relatively stable bound state, i.e. the β5-talin and β6-talin complexes (Figure S5, gray), showed a slight increase in buried hydrophobic area during the simulation, yet the area remained smaller than in the 3G9W-based simulations of β1A and β1D. The entropy-driven hydrophobic effect may thus be of lesser importance for the mechanical stability, in agreement with earlier studies [79-81]. However, reliable estimation of entropic contribution under applied mechanical force would require extensive validation and is beyond the scope of the current study.

Backbone hydrogen bonding and conserved tryptophan are important for mechanic stability

All published talin-integrin complex structures [15, 55, 61] share a close contact between D740(β3) and W359(tal) backbones, and their Cα-Cα distance varies between 5.1 Å (2H7E [15]) and 6.1 Å (3G9W [55]). Our analysis of the

Cα-Cα distance for D740(β3) and W359(tal) showed two pronounced peaks (Figure 2 B) that correspond to bound states with one or two backbone hydrogen bonds between the two residues. The first peak, around 5.6 Å, corresponds to the 2-bond conformation seen in the 1MK7 structure (5.4-5.5 Å), and the second, around 6 Å, to a 3G9W-like 1-bond conformation (5.9-6.1 Å). The backbone hydrogen bonds formed between D740(β3) and talin appeared to be stabilized by the interactions of its neighboring residue, W739(β3). The W739(β3) forms a conserved [15, 55, 61] interaction with talin R358(tal) (Figure 2 A), and together with the D740(β3)-W359(tal) hydrogen bonds it formed a cluster of contacts that appeared to determine the lifetime of the talin-integrin complex. This was also true for β5, in which the tryptophan residue is replaced by a tyrosine (Figure 1). Earlier studies also support the importance of the W739(β3)-R358(tal) interaction: a R358A mutation in talin-1 reportedly reduces the binding of integrin β3 [61, 82], β1A, and β1D [60], and the corresponding mutation in Drosophila abolishes the talin-integrin interaction [83]. Similarly, a W739A mutation has been reported to inhibit β3-integrin to talin-1 [84].

The crystal structure of the β3-talin-1 complex [61] shows that the A742(β3) and K357(tal) residues are sufficiently close to be able to form a third backbone hydrogen bond between talin and β3-integrin. Further analysis of crystal structures shows that the Cα-Cα distance of this residue pair varies between 5.3 Å (1MK7, β3-integrin-talin-1) and 9.9 Å (3G9W: chains B,C; β1D-integrin-talin-2). The 1MK7 structure allows a close contact to form between the A742(β3) and K357(tal) residues, as was observed in many of the longer simulations. This contact was less stable than the D740(β3)-W359(tal) contact, and dissociated before D740(β3)-W359(tal). For example, the corresponding residues in the β5-talin complex, A746(β5) and K357(tal), formed a hydrogen bond that appeared to contribute to the stability of the complex in two long simulations (Table 2). Intriguingly, this A742(β3) position is also the only spot that differs between the β1A and β1D membrane-distal binding site sequences (Figure 1 B). Furthermore, in the 1MK7-based simulations of β1 integrins, the backbone hydrogen bonding between β1D and talin was clearly more force resistant than between β1A and talin (Figure 2 B,C; Figure 4 A,D).

Role of glutamine residue Q778 in the muscle-specific β1D

Integrin β1D reportedly [53, 55, 60, 85] binds more tightly to the talin head compared to β1A. In our 1MK7 structure based simulations, β1A dissociated on average four times as rapidly from talin as β1D (Figure 4). In the 3G9W-based conformation, however, both β1 integrin variants showed a similarly weak force resistance as β1A in the 1MK7 conformation (Figure 2 F). What might then explain the observed higher force resistance of β1D in the 1MK7 conformation?

The crystal structure of the β1D-talin-2 complex [55] shows that integrin β1D binds to talin-2 in a conformation different from that of β3 and talin-1, with Cα RMSD 5.3-5.4 Å for this 14-residue segment of β1D integrin. The differences in integrin backbone conformation bring the integrin into loose contact with talin in terms of backbone hydrogen bonding: the aspartic acid in integrin (β3: D740, β1D: D776) and W359 in talin are bound by two hydrogen bonds in 1MK7, and one in 3G9W.

The Q778(β1D) side chain in 3G9W is oriented towards solution and does not form interactions with talin-2, whereas its counterpart A742(β3) in the 1MK7 structure is buried. In addition, the region between W775(β1D) and the NPxY motif in the β1D in the 3G9W structure is loosely bound, whereas β3 in 1MK7 is in closer contact with talin in this region (Figure 4 A). This difference was also seen with the simulations of β1D: The β1D-3G9W simulations showed no hydrogen bonding between Q778(β1D) and talin-1, whereas in the 1MK7-based simulations, the Q778(β1D) side chain formed a network of hydrogen bonds to T354(tal), I356(tal), and L353(tal) (Figure 4 D-F). Intriguingly, this site in the 1MK7 and 3G9W structures is occupied by the NPxY asparagine (N744 in β3, N780 in β1D), and the NPxY asparagine was also bound in our simulations of the 1MK7-based β1D, β6, and β7. With the combination of backbone and side chain hydrogen bonds via Q778, the 1MK7-based β1D-talin complex was relatively force resistant, but the binding of the NPxY was weak in this conformation (Figure 2 D, F). This may suggest that in β1D, the Q778 side chain can occupy the binding site of the NPxY asparagine N780(β1D) (Figure 4 E), and thus drive the NPxY motif to dissociate from its binding groove.

The mechanical stability of NPxY motif binding varies between integrins and their conformations

The NPxY motif showed weak binding in our simulations: in all 1MK7-based systems the motif dissociated before hydrogen bonds between the D740(β3) and W359(tal) were broken. In the β1A-3G9W and β1D-3G9W simulations, on the other hand, binding of the NPxY motif was more stable than in the 1MK7-based β1 simulations (Figure 2 D, F). This implies that in the 3G9W conformation, the NPxY motif dominates the binding, but does not provide as high force resistance as the D776(β1)-W359(tal) backbone hydrogen bonding in the 1MK7 conformation.

This first NPxY motif in β-integrins is reportedly important for talin binding: mutation of Y783(β1) in β1A or β1D to alanine reduces talin binding [60], and the same mutation to Y759(β7) in β7 abolishes it completely [56]. However, mutation of this tyrosine to alanine has a milder effect on talin binding affinity in β3 than in β1A and β1D [60], and structural analysis shows diversity in how the tyrosine is inserted in its binding site [55, 60, 61]. Our results thus suggest a most intriguing possibility: While the NPxY motif is important for the formation of the talin-integrin complex, its contribution to the force resistance of the complex may be considerably smaller. Moreover, it might be possible for the NPxY motif to interact with other integrin adaptors, such as filamin [64, 86], while integrin still remains complexed with talin.

β6-integrin binds talin

While majority of the talin-β6-integrin complexes analyzed under mechanical stress showed similarly poor stability as talin-β1A-integrin, one of the 200 pN simulations of the talin-β6-integrin complex produced a tightly bound conformation (Figure 5). This complex was characterized by a stable (over 60% of the time in on-state) backbone hydrogen bonding pattern of Q734(β6)-W359(tal), A361(tal)-K732(β6), W359(tal)-T735(β6), and T737(β6)-K357(tal) (Table 2, Figure 5). The NPxY tyrosine Y741(β6) did not form stable interactions to its binding groove, and a dynamic salt bridge connected the R742(β6) to D372(tal).

To experimentally confirm that β6-integrin can indeed bind to talin, we immobilized his-tagged talin head on a Ni-NTA surface and studied the binding of streptavidin-conjugated biotinylated integrin peptides. The biosensor data was analyzed by subtracting the signal obtained for peptide-free streptavidin analyzed simultaneously with peptide-conjugated streptavidins. Biosensor experiment revealed β6 showing clearly more binding to talin surface as compared to β6-SCR peptide and β3 (Figure 6). The binding on-rate was found to be fast in terms of kinetics, and virtually all the bound streptavidin-peptide conjugate was released from the sensor within few seconds after moving the sensor to bare buffer. These findings suggest that β6-integrin can bind talin *in vitro* with higher affinity than β3.

β6-integrin has to date not been reported to be a talin binding protein. However, the β6-integrin cytoplasmic tail contains the conserved tryptophan and the NPxY motif recognized as important for talin binding (Figure 1 B), and recent studies show that integrin β6 colocalizes with talin-1 at adhesion sites [76] and interacts with kindlin-1 [74]. Integrin αvβ6 reportedly activates latent TGFβ1 by binding to the latency-associated protein (LAP) [78], and the connection to TGFβ1 signaling has been shown for tissue fibrosis [87, 88], acute lung injury [89], pulmonary emphysema [90], and for example colon and cervical squamous cell carcinomas [91, 92]. Moreover, depletion of functional αvβ6 reportedly causes lung emphysema, skin infection, and periodontal disease in mice [72, 90, 93], possibly by interfering with latent TGFβ1 activation [89]. Therefore, understanding also the interactions of the αvβ6 cytoplasmic tail may help to develop therapies for a variety of diseases.

Experimental

Homology modeling and molecular dynamics

Talin-integrin β3 chimera (PDB ID: 1MK7 [61]; chains B and C) was used as a template in homology modeling. Homology modeling was carried out using Homodge in the Bodil Modeling Environment [94]. All models were inspected visually and side-chain rotamers of integrin residues differing in sequence from β3 were manually selected from the rotamer library [95] implemented in Bodil. Side-chain rotamers of K357(tal) and E386(tal), and I396(tal) were adjusted in some of the complexes to allow contact with integrin and to abolish steric clashes.

The obtained models were hydrogenated using Psfgen tool in VMD [96] and moved to a box filled with explicit TIP3 water molecules [97]. Water molecules resolved in 1MK7 were included in the system. Physiological ionic strength and neutral total charge was obtained by adding 150 mM Na^+ and Cl^- ions to the system. The system was then subjected to two 4000-step conjugate gradient energy minimizations with NAMD [98] using the CHARMM22 force field [99], first with all protein atoms fixed, and then with all atoms released to move.

Temperature of the system was gradually increased to 310 K under 1 atm pressure in 31 ps using the Berendsen barostat [100]. The system was then subjected to equilibrium simulations under 310 K constant temperature and 1 atm pressure.

Steered molecular dynamics

To study the force-resistance of the complex, constant force was applied to the complex. Force was applied to the N-terminal Cα atom of the integrin fragment and to the Cα atoms of residues L400(tal), G371(tal) and N355(tal) in talin F3 domain.

The charged group of integrin C-terminus was found to make contacts to integrins β3, β5, and β6 in the SMD simulations. We thus ran a new set of simulations without termini for each of these three complexes to avoid the problem of false ionic contacts at the termini, and the terminus-free data were used for the analyses.

Molecular dynamics data analysis

Hydrogen bonding analysis. The trajectory from NAMD simulation was subjected to hydrogen bonding analysis in VMD. The analysis was based on the script by Anishkin [101], and cutoff values 3.51 Å for donor-acceptor distance and 30.1° for deviation from 180° for the donor-hydrogen-acceptor angle were applied. For on-state percentage calculations of hydrogen bonds, the end of the simulation was defined as the last frame containing at least one hydrogen bond between talin and integrin.

Solvent-buried area of the complex. The area buried from solvent in each talin-integrin complex was calculated with a 1.4 Å scanning probe using the 'sasa' function in VMD. The last 200 frames of the simulations without constant force pulling were used for the analysis. Average and standard deviation were calculated from three simulations for each β-integrin-talin complex.

RMSF calculation. The last 200 frames of the simulations without constant force pulling were used superimposed using the Cα atoms of talin residues 311-395 as a reference. RMSF was calculated for integrin Cα atoms in the 200 frames. Average and standard deviation were calculated from three simulations for each β-integrin-talin complex.

Contact stability. Contact stability along the integrin-talin interface was analyzed using the Cα-Cα distance of β3-integrin D740(β3) and A742(β3) from talin W359(tal) and K357(tal), respectively. In addition, we calculated the distance between the centers of mass of W739(β3) and R358(tal) side chains, and the distance of Y747(β3) side chain center of mass from N355(tal) carbonyl oxygen. For other integrins, the residues at corresponding positions were used. The

distances were collected into histograms using a bin width of 0.2 Å. Bound state lifetimes were estimated by counting the observations of Cα distances within a 7 Å cutoff.

Production of recombinant talin head

The production of his-tagged talin head protein is described in [102]. In brief, his-tagged human talin-head was generated by inserting residues 1-406 of human talin1 into pTrcHisC vector (Life Technologies, Carlsbad, California, United States) at the BamHI site and confirmed by DNA sequencing. The protein was expressed in *E. coli* BL21-Star cells at 37 °C. Lysate was prepared using homogenization (Emulsiflex C3, Avestin Inc. Ottawa, Canada) in 20mM NaPO4, 1M NaCl, 20mM imidazole pH 7.4. After clarification by centrifugation, the lysate was applied on HisTrap FF crude 5 ml affinity column using ÄKTA Purifier (GE Healthcare), washed, and eluted with linear imidazole gradient 0-700 mM. Eluted fractions were further purified by cation exchange chromatography using HiTrap SP FF 1 ml column (GE Healthcare). For this purpose, talin-containing fractions were pooled together and diluted (1:10) in 20mM Tris-HCl 20 mM NaCl pH 7.5 (running buffer). Elution was performed by preparing linear NaCl gradient by mixing running buffer and 20mM Tris-HCl, 1 M NaCl, pH 7.5. Talin head was eluted at around 550 mM NaCl. Fractions containing talin protein were further concentrated through 30K filter and analyzed on SDS-PAGE gel. The protein was estimated to be over 95% pure.

Interaction analysis with Octet biosensor

N-terminally biotinylated and C-terminally amidated β3 (HDRKEFAKFEEERARAKWDTANNPLYKE), β6 (HDRKEVAKFEAERSKAKWQTGTNPLYRG) and scrambled β6 (KDWGTEHRQALNSVYFKAGKERKTPARE) peptides were purchased from Caslo (Lyngby, Denmark). Biosensor analyses were performed by using Fortebio Octet RED384 instrument (Pall, Menlo Park, CA) using Ni-NTA sensors. Temperature of 25°C and stirring speed of 1000 rpm were used throughout the experiment. Sensors were chemically activated by immersing them in 0.1M EDC 0.05M NHS in H_2O for 100 seconds. His-tagged talin head domain (50 µg/ml) was used to biofunctionalize the biosensors in 50 mM $NaPO_3$ 150 mM NaCl pH 7.2, resulting a binding response of ~8 nm after 300 s incubation. The remaining activated groups were then quenched by 1M ethanolamine (pH 8.5) for 100 seconds. Because binding of peptides directly on talin-functionalized surface provided negligible responses, the peptides were first conjugated to streptavidin (Anaspec, Fremont, CA, USA) using molar ratio of 1 peptide per streptavidin tetramer. These conjugates were then applied on talin-functionalized surface in various concentrations and each concentration was assayed for 200 s.

Visualization

Molecular structure details were rendered using PyMOL (Schrödinger, LLC), histograms were prepared with Gnumeric (https://projects.gnome.org/gnumeric), and images were further processed with GIMP (http://www.gimp.org/) and Inkscape (http://www.inkscape.org/). Residues were numbered according to expressed protein sequence without signal peptide (UniProt:P05556-1, β1A; P05556-5, β1D; P05106, β3; P18084, β5; P18564, β6; P26010, β7). Amino acid residue positions in the different β-integrins are referred to using β3 numbering for clarity.

Conclusions

These are the first data from a simulation to predict force resistance in the binding of β-integrin membrane-distal talin-binding stretch to talin, that is, the assumedly first contacts in the process of integrin activation. The results show a diversity of binding conformations for the β-integrin, and underlines the importance of a close talin contact for the peptide between the conserved tryptophan and NPxY motifs in β-integrin. Our findings also suggest the NPxY motif might have a minor role in the force resistance of the talin-integrin complex. Moreover, our data suggest that integrin β6 may bind talin-1 with moderate affinity.

Acknowledgements

We thank the Academy of Finland and Tampere Graduate Program in Biomedicine and Biotechnology (TGPBB) for funding, Dr. Bernhard Wehrle-Haller for comments, and the Swiss Center for Scientific Computing (CSCS), ETH Zurich, and CSC – IT Center for Science Ltd for providing the computational resources for this study. We thank Dr. Stuart Prince for proofreading the manuscript text.

References

1 V. Vogel and G. Baneyx, *Annu. Rev. Biomed. Eng.*, 2003, **5**, 441-463.
2 H. Dobereiner, B. J. Dubin-Thaler, G. Giannone and M. P. Sheetz, *J. Appl. Physiol.*, 2005, **98**, 1542-1546.
3 V. Vogel and M. Sheetz, *Nat. Rev. Mol. Cell Biol.*, 2006, **7**, 265-275.
4 T. Lecuit and P. Lenne, *Nat. Rev. Mol. Cell Biol.*, 2007, **8**, 633-644.
5 J. T. Parsons, A. R. Horwitz and M. A. Schwartz, *Nat. Rev. Mol. Cell Biol.*, 2010, **11**, 633-643.
6 I. Schoen, B. L. Pruitt and V. Vogel, *Annu. Rev. Mater. Res.*, 2013, **43**, 589-618.
7 P. Kanchanawong, G. Shtengel, A. M. Pasapera, E. B. Ramko, M. W. Davidson, H. F. Hess and C. M. Waterman, *Nature*, 2010, **468**, 580-584.
8 M. Vicente-Manzanares and A. R. Horwitz, *J. Cell Sci.*, 2011, **124**, 3923-3927.
9 M. L. Smith, D. Gourdon, W. C. Little, K. E. Kubow, R. A. Eguiluz, S. Luna-Morris and V. Vogel, *PLoS Biol*, 2007, **5**, e268.
10 A. Nicolas, A. Besser and S. A. Safran, *Biophys. J.*, 2008, **95**, 527-539.
11 C. Yu, J. B. K. Law, M. Suryana, H. Y. Low and M. P. Sheetz, *Proc. Natl. Acad. Sci. U. S. A.*, 2011, **108**, 20585-20590.
12 D. A. Calderwood, R. Zent, R. Grant, D. J. G. Rees, R. O. Hynes and M. H. Ginsberg, *J. Biol. Chem.*, 1999, **274**, 28071-28074.
13 O. Vinogradova, A. Velyvis, A. Velyviene, B. Hu, T. A. Haas, E. F. Plow and J. Qin, *Cell*, 2002, **110**, 587-597.
14 M. Kim, C. V. Carman and T. A. Springer, *Science*, 2003, **301**, 1720-1725.
15 K. L. Wegener, A. W. Partridge, J. Han, A. R. Pickford, R. C. Liddington, M. H. Ginsberg and I. D. Campbell, *Cell*, 2007, **128**, 171-182.
16 C. Kim, F. Ye, X. Hu and M. H. Ginsberg, *J. Cell Biol.*, 2012, **197**, 605-611.

17 M. Moser, B. Nieswandt, S. Ussar, M. Pozgajova and R. Fassler, *Nat. Med.*, 2008, **14**, 325-330.

18 Y. Ma, J. Qin, C. Wu and E. F. Plow, *J. Cell Biol.*, 2008, **181**, 439-446.

19 R. O. Hynes, *Cell*, 2002, **110**, 673-687.

20 E. Puklin-Faucher and M. P. Sheetz, *J. Cell. Sci.*, 2009, **122**, 179-186.

21 N. Nishida, C. Xie, M. Shimaoka, Y. Cheng, T. Walz and T. A. Springer, *Immunity*, 2006, **25**, 583-594.

22 J. A. Askari, C. J. Tynan, S. E. D. Webb, M. L. Martin-Fernandez, C. Ballestrem and M. J. Humphries, *J. Cell Biol.*, 2010, **188**, 891-903.

23 X. Zhang, G. Jiang, Y. Cai, S. J. Monkley, D. R. Critchley and M. P. Sheetz, *Nat. Cell Biol.*, 2008, **10**, 1062-1068.

24 S. J. Franco, M. A. Rodgers, B. J. Perrin, J. Han, D. A. Bennin, D. R. Critchley and A. Huttenlocher, *Nat. Cell Biol.*, 2004, **6**, 977-983.

25 D. A. Calderwood, I. D. Campbell and D. R. Critchley, *Nat. Rev. Mol. Cell Biol.*, 2013, **14**, 503-517.

26 G. Jiang, G. Giannone, D. R. Critchley, E. Fukumoto and M. P. Sheetz, *Nature*, 2003, **424**, 334-337.

27 Y. Aratyn-Schaus and M. L. Gardel, *Curr. Biol.*, 2010, **20**, 1145-1153.

28 C. G. Galbraith, K. M. Yamada and M. P. Sheetz, *J. Cell Biol.*, 2002, **159**, 695-705.

29 N. D. Gallant, K. E. Michael and A. J. García, *Mol. Biol. Cell*, 2005, **16**, 4329-4340.

30 J. D. Humphries, P. Wang, C. Streuli, B. Geiger, M. J. Humphries and C. Ballestrem, *J. Cell Biol.*, 2007, **179**, 1043-1057.

31 D. W. Dumbauld, H. Shin, N. D. Gallant, K. E. Michael, H. Radhakrishna and A. J. García, *J. Cell. Physiol.*, 2010, **223**, 746-756.

32 B. Luo, C. V. Carman and T. A. Springer, *Annu. Rev. Immunol.*, 2007, **25**, 619-647.

33 M. Moser, K. R. Legate, R. Zent and R. Fässler, *Science*, 2009, **324**, 895-899.

34 S. J. Shattil, C. Kim and M. H. Ginsberg, *Nat. Rev. Mol. Cell Biol.*, 2010, **11**, 288-300.

35 P. Roca-Cusachs, N. C. Gauthier, A. del Rio and M. P. Sheetz, *Proc. Natl. Acad. Sci. U. S. A.*, 2009, **106**, 16245-16250.

36 N. Q. Balaban, U. S. Schwarz, D. Riveline, P. Goichberg, G. Tzur, I. Sabanay, D. Mahalu, S. Safran, A. Bershadsky, L. Addadi and B. Geiger, *Nat. Cell Biol.*, 2001, **3**, 466-472.

37 H. Wolfenson, A. Bershadsky, Y. I. Henis and B. Geiger, *J. Cell Sci.*, 2011, **124**, 1425-1432.

38 T. D. Pollard and G. G. Borisy, *Cell*, 2003, **112**, 453-465.

39 M. B. Smith, T. Kiuchi, N. Watanabe and D. Vavylonis, *Biophys. J.*, 2013, **104**, 247-257.

40 B. Geiger, J. P. Spatz and A. D. Bershadsky, *Nat. Rev. Mol. Cell Biol.*, 2009, **10**, 21-33.

41 F. Margadant, L. L. Chew, X. Hu, H. Yu, N. Bate, X. Zhang and M. Sheetz, *PLoS Biol*, 2011, **9**, e1001223.

42 S. W. Moore, P. Roca-Cusachs and M. P. Sheetz, *Dev. Cell*, 2010, **19**, 194.

43 V. Hytönen P. and V. Vogel, *PLoS Comput Biol*, 2008, **4**, e24.

44 A. del Rio, R. Perez-Jimenez, R. Liu, P. Roca-Cusachs, J. M. Fernandez and M. P. Sheetz, *Science*, 2009, **323**, 638-641.

45 M. Yao, B. T. Goult, H. Chen, P. Cong, M. P. Sheetz and J. Yan, *Sci. Rep.*, 2014, 4.

46 J. D. Humphries, A. Byron and M. J. Humphries, *J. Cell. Sci.*, 2006, **119**, 3901-3903.

47 F. Altruda, P. Cervella, G. Tarone, C. Botta, F. Balzac, G. Stefanuto and L. Silengo, *Gene*, 1990, **95**, 261-266.

48 A. van der Flier, I. Kuikman, C. Baudoin, R. van der Neut and A. Sonnenberg, *FEBS Lett.*, 1995, **369**, 340-344.

49 A. A. de Melker and A. Sonnenberg, *Bioessays*, 1999, **21**, 499-509.

50 F. J. Conti, S. J. Monkley, M. R. Wood, D. R. Critchley and U. Müller, *Development*, 2009, **136**, 3597-3606.

51 S. J. Monkley, X. Zhou, S. J. Kinston, S. M. Giblett, L. Hemmings, H. Priddle, J. E. Brown, C. A. Pritchard, D. R. Critchley and R. Fässler, *Dev. Dynam.*, 2000, **219**, 560-574.

52 A. Horwitz, K. Duggan, C. Buck, M. C. Beckerle and K. Burridge, *Nature*, 1986, **320**, 531-533.

53 M. Pfaff, S. Liu, D. J. Erle and M. H. Ginsberg, *J. Biol. Chem.*, 1998, **273**, 6104-6109.

54 D. A. Calderwood, A. Huttenlocher, W. B. Kiosses, D. M. Rose, D. G. Woodside, M. A. Schwartz and M. H. Ginsberg, *Nat. Cell Biol.*, 2001, **3**, 1060-1068.

55 N. J. Anthis, K. L. Wegener, F. Ye, C. Kim, B. T. Goult, E. D. Lowe, I. Vakonakis, N. Bate, D. R. Critchley, M. H. Ginsberg and I. D. Campbell, *EMBO J.*, 2009, **28**, 3623-3632.

56 D. A. Calderwood, Y. Fujioka, J. M. de Pereda, B. García-Alvarez, T. Nakamoto, B. Margolis, C. J. McGlade, R. C. Liddington and M. H. Ginsberg, *Proc. Natl. Acad. Sci. U. S. A.*, 2003, **100**, 2272-2277.

57 N. J. Anthis, J. R. Haling, C. L. Oxley, M. Memo, K. L. Wegener, C. J. Lim, M. H. Ginsberg and I. D. Campbell, *J. Biol. Chem.*, 2009, **284**, 36700-36710.

58 F. Saltel, E. Mortier, V. P. Hytönen, M. Jacquier, P. Zimmermann, V. Vogel, W. Liu and B. Wehrle-Haller, *J. Cell Biol.*, 2009, **187**, 715-731.

59 A. C. Kalli, I. D. Campbell and M. S. P. Sansom, *Proc. Natl. Acad. Sci. U. S. A.*, 2011, **108**, 11890-11895.

60 N. J. Anthis, K. L. Wegener, D. R. Critchley and I. D. Campbell, *Structure*, 2010, **18**, 1654.

61 B. García-Alvarez, J. M. d. Pereda, D. A. Calderwood, T. S. Ulmer, D. Critchley, I. D. Campbell, M. H. Ginsberg and R. C. Liddington, *Mol. Cell*, 2003, **11**, 49-58.

62 H. B. Schiller, M. Hermann, J. Polleux, T. Vignaud, S. Zanivan, C. C. Friedel, Z. Sun, A. Raducanu, K. Gottschalk, M. Théry, M. Mann and R. Fässler, *Nat. Cell Biol.*, 2013, **15**, 625-636.

63 G. L. Lin, D. M. Cohen, R. A. Desai, M. T. Breckenridge, L. Gao, M. J. Humphries and C. S. Chen, *FEBS Lett.*, 2013, **587**, 763-769.

64 K. R. Legate and R. Fässler, *J. Cell Sci.*, 2009, **122**, 187-198.

65 C. J. McCleverty, D. C. Lin and R. C. Liddington, *Protein Sci.*, 2007, **16**, 1223-1229.

66 V. Vogel and M. P. Sheetz, *Curr. Opin. Cell Biol.*, 2009, **21**, 38-46.

67 R. Zaidel-Bar and B. Geiger, *J. Cell. Sci.*, 2010, **123**, 1385-1388.

68 P. Roca-Cusachs, A. del Rio, E. Puklin-Faucher, N. C. Gauthier, N. Biais and M. P. Sheetz, *Proc. Natl. Acad. Sci. U. S. A.*, 2013, **110**, E1361-E1370.

69 T. Kiema, Y. Lad, P. Jiang, C. L. Oxley, M. Baldassarre, K. L. Wegener, I. D. Campbell, J. Ylänne and D. A. Calderwood, *Mol. Cell*, 2006, **21**, 337-347.

70 J. M. Breuss, N. Gillett, L. Lu, D. Sheppard and R. Pytela, *J. Histochem. Cytochem.*, 1993, **41**, 1521-1527.

71 J. M. Breuss, J. Gallo, H. M. DeLisser, I. V. Klimanskaya, H. G. Folkesson, J. F. Pittet, S. L. Nishimura, K. Aldape, D. V. Landers and W. Carpenter, *J. Cell Sci.*, 1995, **108**, 2241-2251.

72 X. Z. Huang, J. F. Wu, D. Cass, D. J. Erle, D. Corry, S. G. Young, R. V. Farese and D. Sheppard, *J. Cell Biol.*, 1996, **133**, 921-928.

73 A. Bandyopadhyay and S. Raghavan, *Curr. Drug Targets*, 2009, **10**, 645-652.

74 A. Bandyopadhyay, G. Rothschild, S. Kim, D. A. Calderwood and S. Raghavan, *J. Cell Sci.*, 2012, **125**, 2172-2184.

75 D. S. Harburger, M. Bouaouina and D. A. Calderwood, *J. Biol. Chem.*, 2009, **284**, 11485-11497.

76 D. W. Erikson, R. C. Burghardt, K. J. Bayless and G. A. Johnson, *Biol. Reprod.*, 2009, **81**, 814-825.

77 P. Wipff, D. B. Rifkin, J. Meister and B. Hinz, *J. Cell Biol.*, 2007, **179**, 1311-1323.

78 J. S. Munger, X. Huang, H. Kawakatsu, M. J. D. Griffiths, S. L. Dalton, J. Wu, J. Pittet, N. Kaminski, C. Garat, M. A. Matthay, D. B. Rifkin and D. Sheppard, *Cell*, 1999, **96**, 319-328.

79 H. Lu, B. Isralewitz, A. Krammer, V. Vogel and K. Schulten, *Biophys. J.*, 1998, **75**, 662-671.

80 H. Lu and K. Schulten, *Proteins*, 1999, **35**, 453-463.

81 M. Carrion-Vazquez, A. F. Oberhauser, T. E. Fisher, P. E. Marszalek, H. Li and J. M. Fernandez, *Prog. Biophys. Mol. Biol.*, 2000, **74**, 63-91.

82 S. Tadokoro, S. J. Shattil, K. Eto, V. Tai, R. C. Liddington, J. M. d. Pereda, M. H. Ginsberg and D. A. Calderwood, *Science*, 2003, **302**, 103-106.

83 G. Tanentzapf and N. H. Brown, *Nat. Cell Biol.*, 2006, **8**, 601-606.

84 D. A. Calderwood, V. Tai, G. Di Paolo, P. De Camilli and M. H. Ginsberg, *J. Biol. Chem.*, 2004, **279**, 28889-28895.

85 A. M. Belkin, S. F. Retta, O. Y. Pletjushkina, F. Balzac, L. Silengo, R. Fassler, V. E. Koteliansky, K. Burridge and G. Tarone, *J. Cell Biol.*, 1997, **139**, 1583-1595.

86 M. Das, S. Subbayya Ithychanda, J. Qin and E. F. Plow, *BBA-Biomembranes*, 2014, **1838**, 579-588.

87 K. Hahm, M. E. Lukashev, Y. Luo, W. J. Yang, B. M. Dolinski, P. H. Weinreb, K. J. Simon, L. Chun Wang, D. R. Leone, R. R. Lobb, D. J. McCrann, N. E. Allaire, G. S. Horan, A. Fogo, R. Kalluri, C. F. Shield III, D. Sheppard, H. A. Gardner and S. M. Violette, *Am. J. Pathol.*, 2007, **170**, 110-125.

88 K. Puthawala, N. Hadjiangelis, S. C. Jacoby, E. Bayongan, Z. Zhao, Z. Yang, M. L. Devitt, G. S. Horan, P. H. Weinreb, M. E. Lukashev, S. M. Violette, K. S. Grant, C. Colarossi, S. C. Formenti and J. S. Munger, *Am. J. Respir. Crit. Care Med.*, 2008, **177**, 82-90.

89 J. Pittet, M. J. D. Griffiths, T. Geiser, N. Kaminski, S. L. Dalton, X. Huang, L. A. S. Brown, P. J. Gotwals, V. E. Koteliansky, M. A. Matthay and D. Sheppard, *J. Clin. Invest.*, 2001, **107**, 1537-1544.

90 D. G. Morris, X. Huang, N. Kaminski, Y. Wang, S. D. Shapiro, G. Dolganov, A. Glick and D. Sheppard, *Nature*, 2003, **422**, 169-173.

91 R. C. Bates, D. I. Bellovin, C. Brown, E. Maynard, B. Wu, H. Kawakatsu, D. Sheppard, P. Oettgen and A. M. Mercurio, *J. Clin. Invest.*, 2005, **115**, 339-347.

92 S. Hazelbag, G. Kenter, A. Gorter, E. Dreef, L. Koopman, S. Violette, P. Weinreb and G. Fleuren, *J. Pathol.*, 2007, **212**, 316-324.

93 F. Ghannad, D. Nica, M. I. Garcia Fulle, D. Grenier, E. E. Putnins, S. Johnston, A. Eslami, L. Koivisto, G. Jiang, M. D. McKee, L. Häkkinen and H. Larjava, *Am. J. Pathol.*, 2008, **172**, 1271-1286.

94 J. Lehtonen, D. Still, V. Rantanen, J. Ekholm, D. Björklund, Z. Iftikhar, M. Huhtala, S. Repo, A. Jussila, J. Jaakkola, O. Pentikäinen, T. Nyrönen, T. Salminen, M. Gyllenberg and M. Johnson, *J. Comput. Aid. Mol. Des.*, 2004, **18**, 401-419.

95 S. C. Lovell, J. M. Word, J. S. Richardson and D. C. Richardson, *Proteins*, 2000, **40**, 389-408.

96 W. Humphrey, A. Dalke and K. Schulten, *J. Mol. Graph.*, 1996, **14**, 33-38.

97 W. L. Jorgensen, J. Chandrasekhar, J. D. Madura, R. W. Impey and M. L. Klein, *J. Chem. Phys.*, 1983, **79**, 926-935.

98 J. C. Phillips, R. Braun, W. Wang, J. Gumbart, E. Tajkhorshid, E. Villa, C. Chipot, R. D. Skeel, L. Kalé and K. Schulten, *J. Comput. Chem.*, 2005, **26**, 1781-1802.

99 MacKerell A. D., D. Bashford, Bellott, Dunbrack R. L., J. D. Evanseck, M. J. Field, S. Fischer, J. Gao, H. Guo, S. Ha, D. Joseph-McCarthy, L. Kuchnir, K. Kuczera, F. T. K. Lau, C. Mattos, S. Michnick, T. Ngo, D. T. Nguyen, B. Prodhom, W. E. Reiher, B. Roux, M. Schlenkrich, J. C. Smith, R. Stote, J. Straub, M. Watanabe, J. Wiórkiewicz-Kuczera, D. Yin and M. Karplus, *J. Phys. Chem. B*, 1998, **102**, 3586-3616.

100 H. J. C. Berendsen, J. P. M. Postma, W. F. v. Gunsteren, A. DiNola and J. R. Haak, *J. Chem. Phys.*, 1984, **81**, 3684-3690.

101 A. Anishkin and S. Sukharev, *Biophys. J.*, 2004, **86**, 2883-2895.

102 P. Pinon, J. Pärssinen, P. Vazquez, M. Bachmann, R. Rahikainen, M. Jacquier, L. Azizi, J. A. Määttä, M. Bastmeyer, V. P. Hytönen and B. Wehrle-Haller, *J. Cell Biol.*, 2014, **205**, 265-281.

103 R. C. Edgar, *Nucleic Acids Res.*, 2004, **32**, 1792-1797.

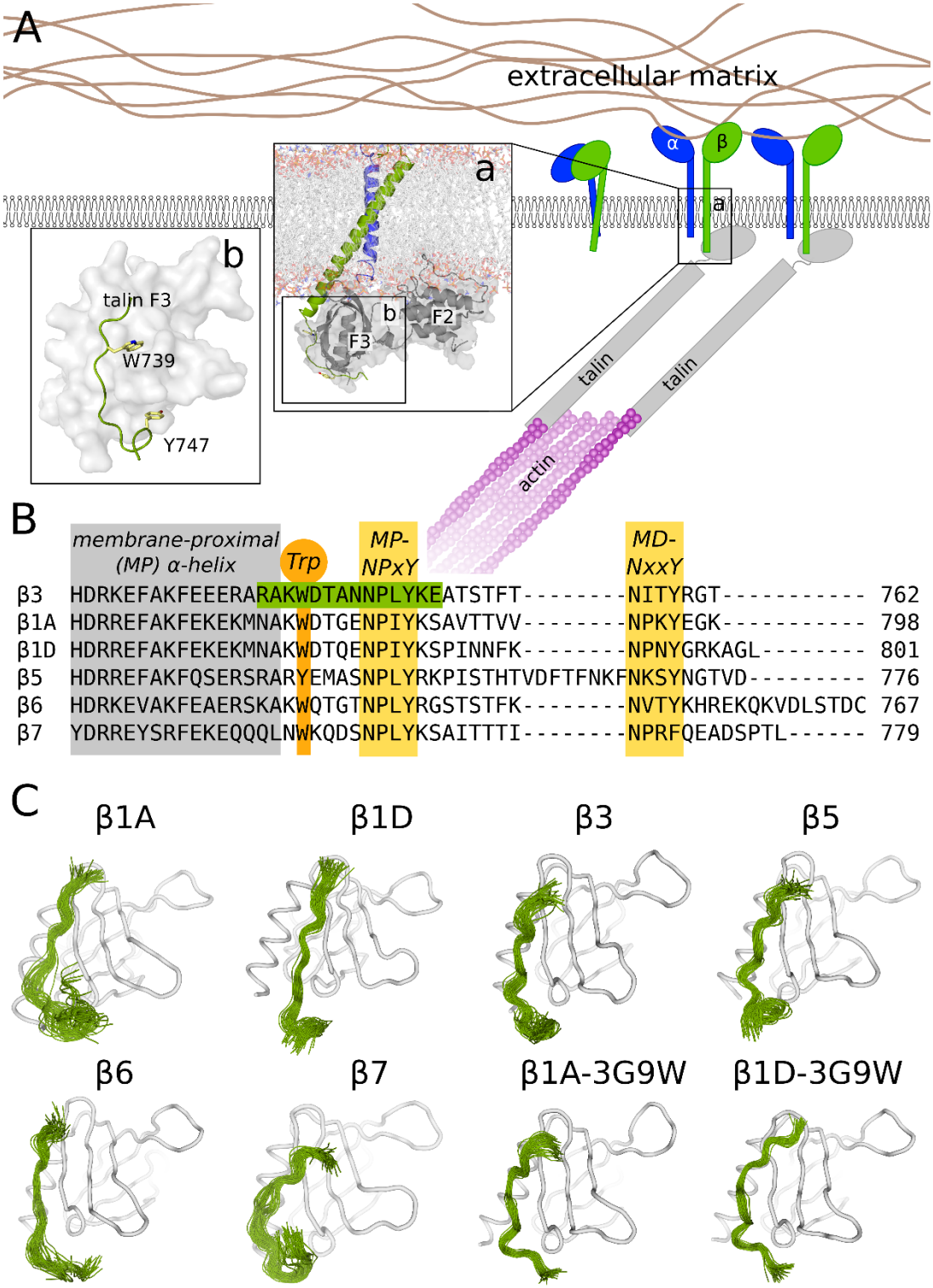

Figure 1 A: Schematic representation of the talin-integrin complex at the cell membrane. Focal adhesions connect the extracellular matrix (ECM) to the actin cytoskeleton (purple) through an integrin heterodimer. Talin binds to the cytoplasmic tail of β-integrin in the early steps of focal adhesion formation. Several other proteins contribute to the signaling and functional diversity at adhesion sites. a) Talin-integrin complex at a lipid bilayer. Talin subdomains F2 and F3 are shown in gray, and integrin β3 cytoplasmic tail in green. Figure rendered using the model of αIIbβ3/β1D chimeric integrin and talin-2 published by Kalli and coworkers [59]. b) A closer view of talin-1 F3-subdomain in complex with β3-integrin in the 1MK7 structure. B: β-integrin cytoplasmic domains aligned using MUSCLE 3.8 [103]. The sequence stretch used in the simulations is highlighted with green in the sequence of the structural template of the models, integrin β3. The conserved tryptophan residue (tyrosine in β5) is labeled as Trp. The talin-binding membrane-proximal (MP) NPxY motif and the membrane-distal (MD) NxxY motif are highlighted in yellow. Residue numbers are provided for the C-terminal residues. C: Dynamics of the of the integrin tail docked to the F3 domain of talin. Main chain presentation of integrins (green) shown every 5 ps in the last 200 ps before starting the SMD simulations.

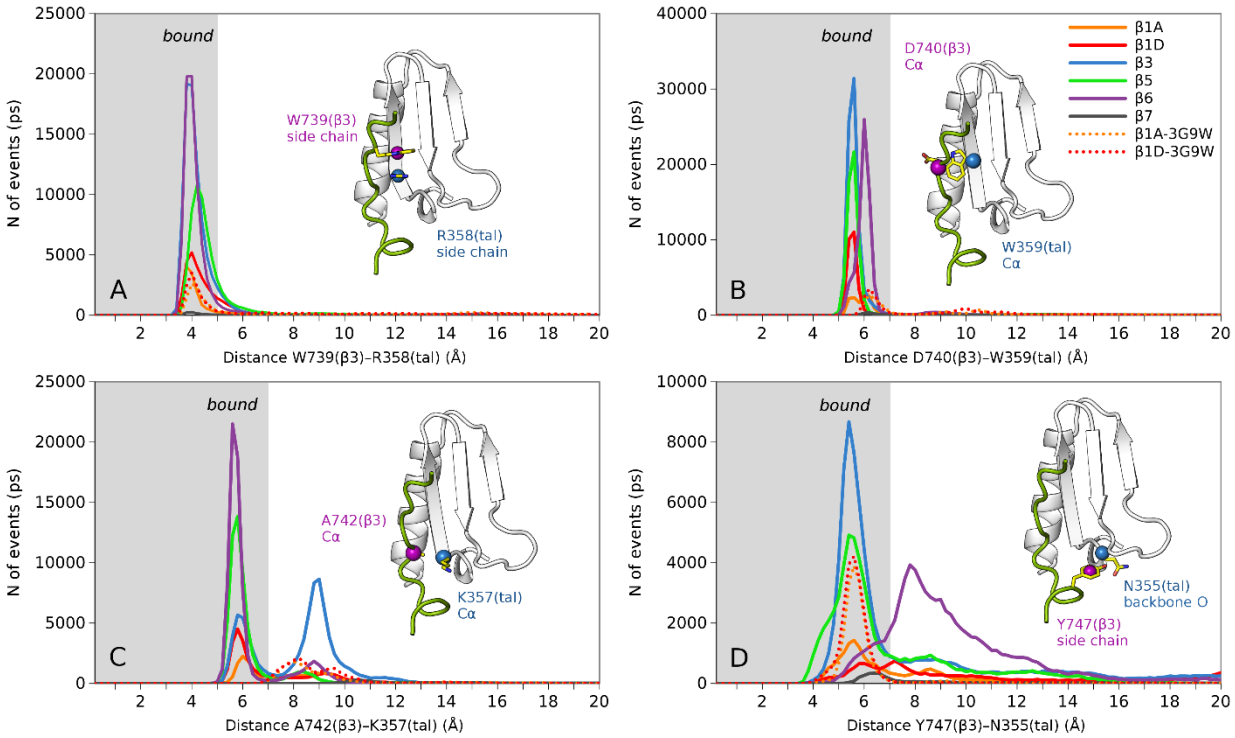

Figure 2 Talin-integrin distances along the binding interface in the simulations. Solid lines: simulations based on the β3-talin-1 structure (1MK7). Dashed lines: simulations based on the β1D-talin-2 structure (3G9W). Distances between two residues in four contacts (A-D) are shown as histograms using a bin width of 0.2 Å. The atoms or centers of mass used in distance measurement are shown in the 1MK7 structure, with a purple sphere representing the measuring point in integrin (green) and a blue sphere representing the measuring point in talin (white). The definition of the bound state shown in Figures S1-S4 is highlighted with gray. A: Histogram of distances between the side chain centers of mass of the conserved tryptophan W739(β3) (Y743 in β5) and R358(tal). B: Histogram of Cα-Cα distances between D740(β3) and W359(tal). C: Histogram of Cα-Cα distances between A742(β3) and K357(tal). D: Histogram of distances between NPxY tyrosine side chain center of mass and N355(tal) backbone oxygen atom.

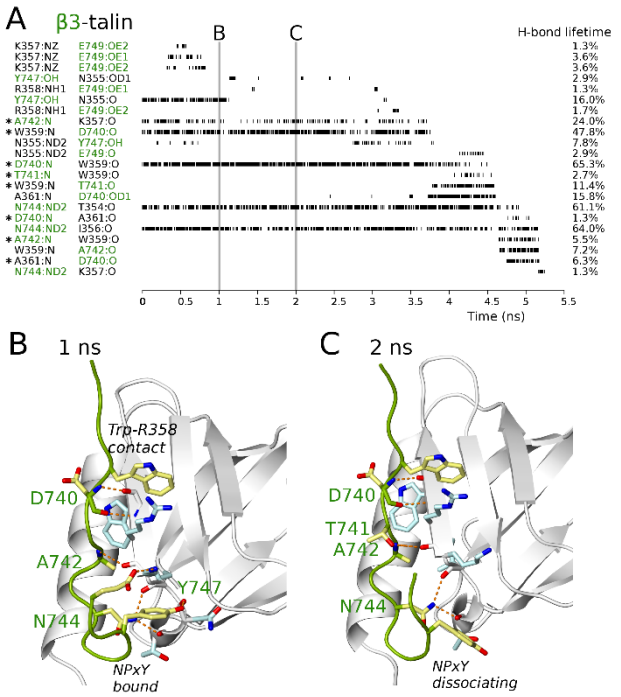

Figure 3 β3-integrin-talin complex in a representative 300 pN SMD simulation. A: Dynamics of hydrogen bond formation and breakage between integrin β3 and talin. The hydrogen bonds were determined every 5 ps using cutoff angle and distance constraints of 30.1° and 3.51 Å, respectively. Hydrogen bonds in on-state are indicated as black bars. Left: donor-acceptor atom pair, integrin in green and talin in black. Hydrogen bonds formed by main chain atoms are marked with *. An on-state percentage for each hydrogen bond is shown on the right. Snapshots (B-C) from the simulation illustrate the hydrogen bonding interactions at 1 ns and 2 ns. Green: main chain presentation of integrin. White: talin shown as cartoon model.

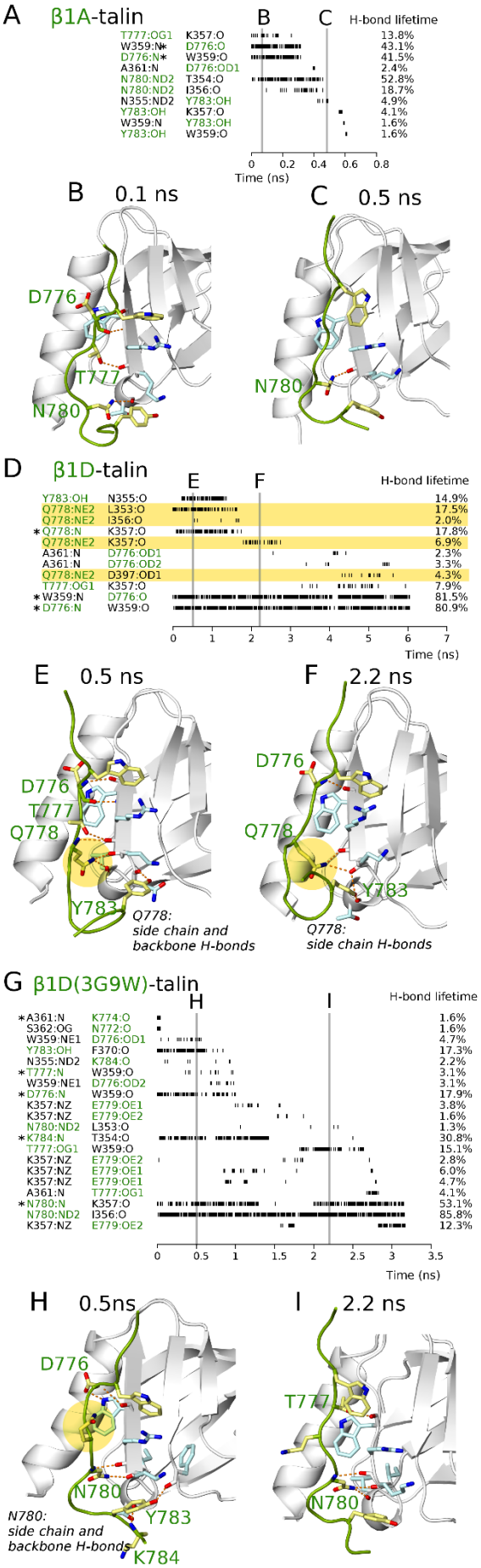

Figure 4 Hydrogen bonding of β1 variants to talin in representative 300 pN constant force pulling simulations. A: Illustration of the crystal structures used as templates for β1A (1MK7), β1D (1MK7), and β1D-3G9W simulations (3G9W). Simulations of complexes based on the 1MK7 are shown in A-C (β1A) and D-F (β1D). A simulation of β1D based on the 3G9W structure is shown in G-I. Hydrogen bonds were determined once every 5 ps (β 1A) or 10 ps (β1D, β1D-3G9W) and plotted in A, D, and G. Yellow color highlights residue Q778(β1D) in the β1D panels. Left: donor-acceptor atom pair, integrin in green and talin in black. Hydrogen bonds formed by main chain atoms are marked with *. An on-state percentage for each hydrogen bond is shown on the right. Snapshots (B-C, E-F, H-I) from the simulations illustrate the hydrogen bonding interactions at the marked time points. Green: main chain presentation of integrin. White: talin shown as cartoon model. Integrin residues contributing to hydrogen bonding with talin are labeled.

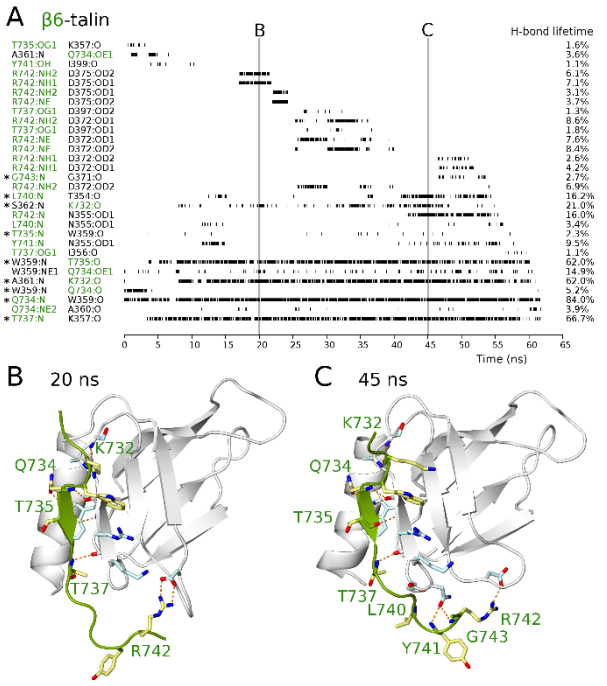

Figure 5 Hydrogen bonding and snapshots in a 200 pN simulation of β6-integrin and talin. Left: donor-acceptor atom pair, integrin in green and talin in black. Hydrogen bonds formed by main chain atoms are marked with *. An on-state percentage for each hydrogen bond is shown on the right. Snapshots (B-C) from the simulations illustrate the hydrogen bonding interactions at the marked time points. Green: main chain presentation of integrin. White: talin shown as cartoon model. Integrin residues contributing to hydrogen bonding with talin are labeled.

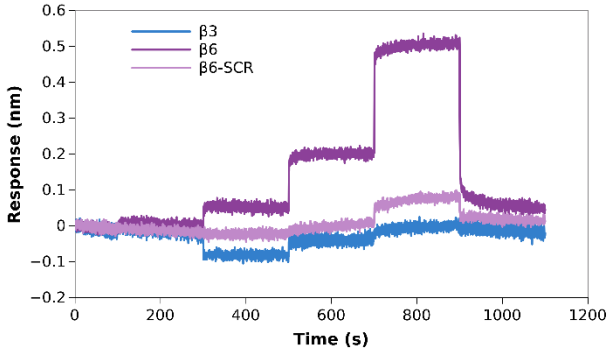

Figure 6 Octet biosensor analysis for talin-integrin binding. Ni-NTA biosensor covalently functionalized with His-tagged talin head was used to analyze the binding to various integrin tails. N-terminally biotinylated peptides corresponding to C-terminally truncated cytoplasmic domains of β3 and β6 were conjugated to streptavidin and applied on the biosensor surface in concentrations indicated in the figure. 0-100 s, baseline; 100-300 s, 1.8 μM; 300-500 s, 7.3 μM; 500-700 s, 29.4 μM; 700-900 s, 117.5 μM. The biosensor was then moved back to the buffer containing no protein in order to visualize the dissociation of the complex (900-1100 s).

Table 1 Characteristics of talin head-integrin tail complexes in the 1-ns simulations before starting the constant force pulling simulations. A_{buried}: buried area. H-bonds: number of hydrogen bonds. RMSF: root mean square fluctuation for integrin Cα atoms. SD: standard deviation. The β3-talin complex originated from the crystal structure 1MK7, and was used as a template in the homology modeling of the other complexes.

Integrin	A_{buried} ±SD (Å^2)	H-bonds ±SD	RMSF ±SD (Å)
β1A	571 ± 38	4.1 ± 1.4	2.25 ± 0.55
β1D	564 ± 53	3.7 ± 1.4	1.76 ± 0.34
β3	601 ± 33	4.4 ± 1.3	1.85 ± 0.35
β5	642 ± 65	4.6 ± 2.2	1.82 ± 0.53
β6	579 ± 69	2.8 ± 1.0	2.02 ± 0.49
β7	514 ± 66	2.0 ± 1.1	2.12 ± 0.30
β1A-3G9W	749 ± 46	4.1 ± 1.4	1.03 ± 0.21
β1D-3G9W	790 ± 58	4.5 ± 1.7	1.08 ± 0.24

Table 2 Lifetimes (ns) of selected stable talin-integrin hydrogen bonds from the simulations. β3-integrin numbering is used for the residues of all integrins. Side chains participating in hydrogen bonding are marked with "sc".

H-bond	β3 (200 pN)	β3 (200 pN)	β5 (200 pN)	β5 (300 pN)	β6 (200 pN)
D740-W359	30.0	34.1	28.3	14.6	52.3
W359-D740	30.6	28.3	27.2	14.6	-
A742-K357	-	-	22.2	9.5	-
A361-K738	-	-	-	-	38.6
W359-T741	-	-	-	-	39.8
T743-K357	-	-	-	-	42.5
N744(sc)-T354	-	-	-	13.4	-
N744(sc)-I356	-	-	-	11.5	-